American Journal of Condensed Matter Physics 2017, 7(1): 6-16
DOI: 10.5923/j.ajcmp.20170701.02

AC Impedance Response and Electrical Conduction Mechanism of Thin Selenium Films Doped with Samarium Atoms

Fathy A. Abdel-Wahab*, Heba Abdel Maksoud

Physics Department, Faculty of Science, Ain Shams University, Cairo, Egypt

Abstract The dielectric parameters of Sm doped Se films (namely $SeSm_{0.008}$) films prepared by thermal evaporation were measured under vacuum in a wide range of frequency and temperature. The measured real part of the admittance (Y') versus frequency (f) were analyzed and shows two distinct regions. In the first one which lie in the low frequency range Y' displayed an independence on the frequency that give a direct evidence for the existence of Debye model. In the high frequency part, which is considered using power low: $Y' \alpha \omega^n$ ($n \leq 1.0$), a deviation from Debye model is observed where Y' increase linearly against frequency. Analysis of the calculated values of n with reference to those numerically calculated for different theoretical a.c. conduction models shows that correlated barrier hopping (CBH) is a fairly good to describe the dominant conduction mechanism. The equivalent circuit approach is applied by comparing the theoretical and experimental data trends of the plots of Z'-Z'' and Y'-Y'' as function of frequency for all proposed equivalent circuits and showed that $R \| C$ connected in series with $R \| C \|$ CPE is the most appropriate circuit to represent the structure of the investigated films. Furthermore, the dc conductivity calculated using the obtained values of the resistances, R, versus temperature are plotted and discussed according to the current dc conduction theories.

Keywords Se doped Sm, Se doped rare earth, Thin films, Equivalent circuit approach, Impedance spectroscopy, Electrical admittance

1. Introduction

Elemental Selenium is considered to be the most interesting chalcogen in its amorphous (a-) and crystalline (c-) forms. The structure of a-Se consists of randomly distributed rings (Se_8) and polymeric chains (Se_n) molecular units. The filled lone pair (LP) p of Selenium states forms the bonding (s) band while the empty anti-bonding p states form anti-bonding (s*) band. The valence band of Se is formed from the lone pair p electrons and the valence s states of Se lie far below the top of the valence band [1]. During crystallization, the chains of Se_n and Se_8 rings transforms into hexagonal and monoclinic structure in sequence.

On the other hand Samarium rare earth element characterizes by the presence of 4f states which are fully occupied and locate in the energy gap between chalcogen 3p and Sm 5d states. In Samarium mono-selenide these 4f states forms together with the conduction band of a-Se the new conduction band of Sm mono-selenide [3, 4]. These structural modifications of Se due to doping with Sm change its basic properties that make it a promising candidate for pressure sensor [5] and thermoelectric power converters [6].

Impedance spectroscopy (IS) is a powerful technique used to extract and analyze the electrical properties for a wide variety of materials ranging from insulators to superconductors [7, 8]. These properties could be argued to the structural network such as: i) intra-granular (grain or bulk), ii) inter-granular (grain boundaries), iii) combination of grains and grain boundaries and iv) interfaces and conducting electrodes. According to this technique the different structural regions in the material could be theoretically separated to find the impedance of each region. Furthermore, the impedance could be analyzed into its real (resistive) and imaginary (capacitive) parts. To extract this information, it is essential to model experimental data using an equivalent electrical circuit, i.e. some combination of resistors, capacitors, and in sometimes, constant phase elements (CPEs) that give the same impedance response as the studied material. The values of these components depend on the applies frequency and temperature [9, 10].

In the previous work [11, 12], the electrical conduction and dielectric relaxation in bulk and thin film crystalline Se doped with 0.005 of Sm have been studied. In the present work, The dependence of the real part of admittance, Y' on

* Corresponding author:
fabdelwahab@sci.asu.edu.eg (Fathy A. Abdel-Wahab)
Published online at http://journal.sapub.org/ajcmp

frequency, for $SeSm_{0.008}$ films, illustrated presence of dc region in the low frequency followed by ac region in the high frequency part which is analyzed using power law of the form $Y' \alpha \omega^n$ ($n \leq 1.0$). A comparison between the values of the index *n* calculated using equivalent circuit approach and different a.c. conduction mechanism are used to explore the most probable conduction mechanism in the investigated films. Furthermore, the obtained values of the resistances for the studied samples using equivalent circuit approach are used in order to account for the dc conductivity and its dependence on temperature.

2. Experimental Details

Bulk selenium doped Samarium of the composition $SeSm_{0.008}$ was prepared by mixing appropriate proportions of Se and Sm, of purity 5 N, in a silica tube sealed at 10^{-5} Torr. The mixture was heated in an electric furnace at rate of ~200 ℃ h^{-1} to 950 ℃ and kept at that temperature for 9 h. The obtained bulk ingots of composition $SeSm_{0.008}$ were used as source material to prepare thin films by the thermal evaporation technique. More details about preparation and electrical measurements of bulk and thin film Se doped Sm is given elsewhere [11, 12]. After evaporation, the thickness of the fresh films was accurately determined by an optical interference method and is found to be 820 nm.

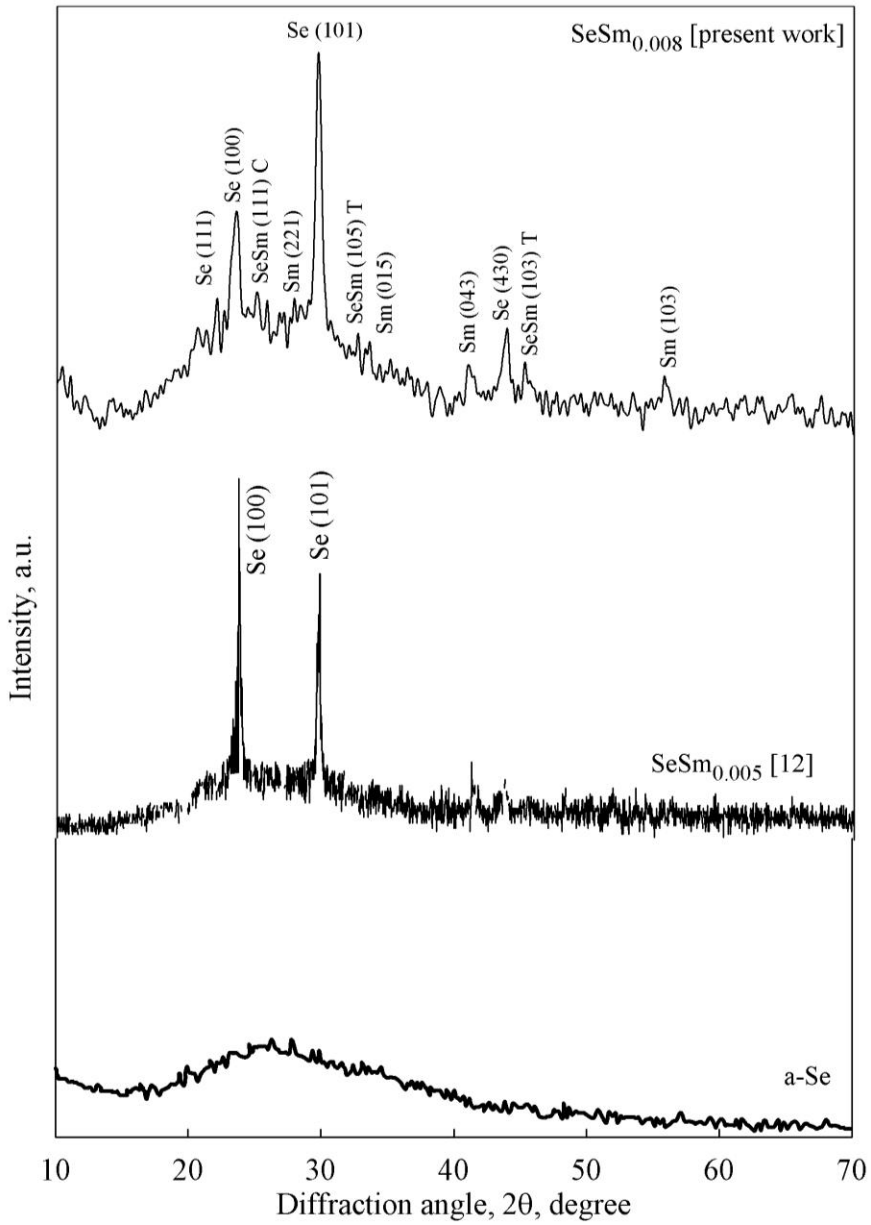

Figure (1). XRD pattern of a-Se, $SeSm_{0.005}$ [12] and $SeSm_{0.008}$ (present work) films prepared by thermal evaporation. The pattern shows the amorphous character for a-Se while for $SeSm_{0.005}$, the spectrum illustrates also the amorphous nature with presence of some crystallites zones. Furthermore, the polycrystalline nature of $SeSm_{0.008}$ is shown

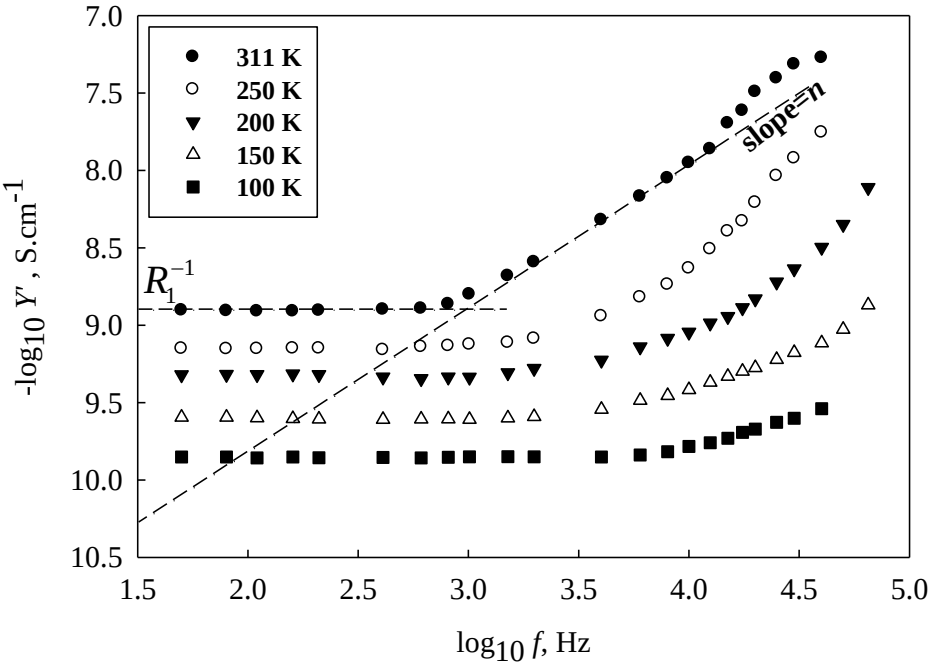

Figure (2). Spectroscopic plot of log $Y^{'}$ against log f at different isotherms. The plot illustrates that at each temperature there are two distinct regions at low and a high frequency for the studied films

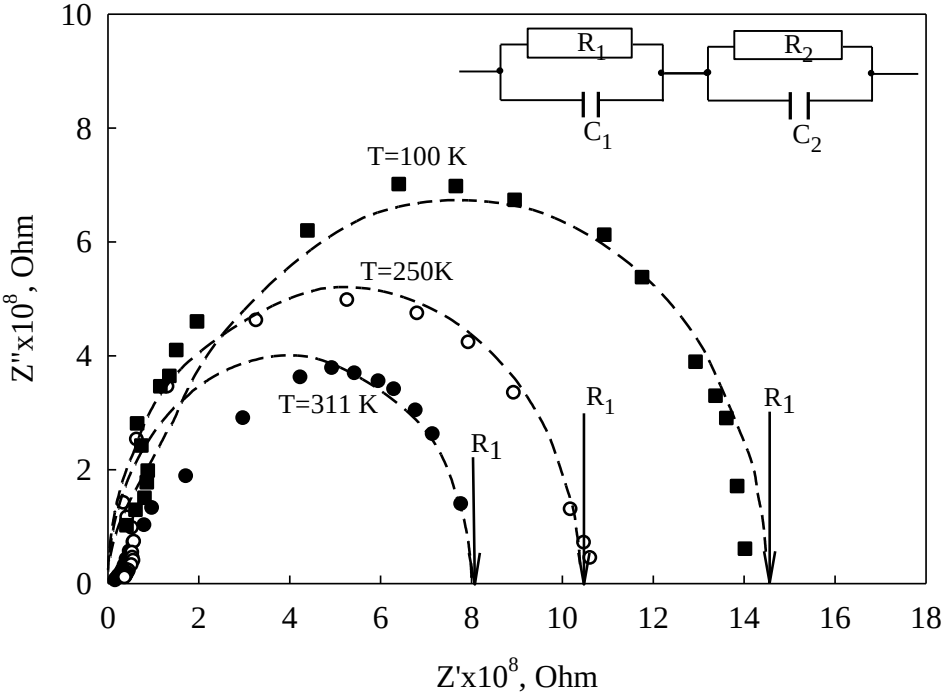

Figure (3). The impedance spectrum of the investigated films at 100, 250 and 311 K in the complex plane. The symbols correspond to experimental data while dashed lines represent the fitting using the equivalent circuit shown in the inset

3. Results and Discussion

The recorded XRD patterns for the studied as-prepared un-doped and Sm doped Se samples are shown in figure (1). In this figure, the XRD pattern of the fresh Se films reflects its amorphous nature. The recorded XRD pattern of the doped a-Se with 0.005 at. % of Sm [12] indicate an amorphous matrix embedded with some crystalline zones.

Furthermore, the XRD pattern of the present a-Se doped with 0.008 at. % of Sm illustrates that the deposited films are polycrystalline in nature and consists of mixed phases of elemental Se (111), (100), (101), (430), elemental Sm (221), (015), (043), (103) and SeSm with cubic (111) and tetragonal (105), (103) structures. The former cubic structure of SeSm has been recorded by other authors [13, 14] for Sm mono-selenides.

3.1. Dispersion of the Electrical Admittance

In ac electrical conductivity, semiconductors exhibit a peculiar dependence on frequency as shown in Fig. (2). This figure demonstrate the real part of the admittance, *Y'* as function of frequency, *f*, plotted at isotherms 311, 250, 200, 150 and 100 K. It should be noted that, for clarification purpose, not all the recorded temperature data points are depicted in the figure.

In the spectroscopic plot of Fig. (2) and at low frequency range, log *Y'* shows a frequency independent plateau (dc component) followed by a "cross over" region to high frequency dispersion (ac component) where log *Y'* increases linearly with log *f*. Indeed, the width of the two regions depends mainly on the applied temperature. In the low frequency region and at high temperature (311 K) the independence region of *Y'* on the frequency *f* is a narrow (50 - 600 Hz) and becomes a wider and more pronounced (0.05 - 4.0 KHz) as temperature decreases (100 K). Furthermore, the independence of *Y'* on the frequency indicates that the investigated films obeys Debye model which means that the micro-structure of the studied films, in this region, could be represented by a single parallel *RC* elements with complex impedance, *Z** and admittance *Y** given by [15]:

$$Y^* = (Z^*)^{-1} = R^{-1} + j\omega C \tag{1}$$

where *R* is the ohmic resistance, ω the angular frequency ($\omega=2\pi f$), *C* is the capacitance and $j=\sqrt{-1}$.

Furthermore, in the low frequency range and at each temperature the function log *Y'* against log *f* are fitted locally point by point to horizontal linear regression line. The extrapolation of the fitted line intersect *Y'* -axis to give the reciprocal of the initial value of the dc resistance (R_1) of the studied sample [15].

In the high frequency region of Fig. (2), the admittance increases linearly against the frequency indicating the deviation of the impedance data from ideal 'Debye like' behavior. In order to model non-ideal IS data of this region, a constant phase element (CPE) is used in addition to resistor and capacitance. The impedance of CPE (Z^*_{CPE}) is defined as [10]:

$$Z^*_{CPE} = [A(j\omega)^n]^{-1} \tag{2}$$

where *A* is a temperature dependent constant and *n* = (dlog*Y'*(*f*)/dlog*f*) while $\log[A\cos(n\pi/2)]$ is the extrapolated intercept with the log *Y'* axis.

The value of *n* ($0 \le n \le 1$) serves as evidence for the type of the dominant ac conduction mechanism in the studied material [16, 7]. The equivalent circuit model enables to analyze and characterize electrically different active regions in the studied material in which the responses of these regions could be deconvoluted and characterized separately. The equivalent circuits are composed of combinations of the impedances of the different structural regions of the studied material besides the CPE in case of deviation from Debye's model.

3.2. Evaluating the Initial Values of Impedances of the Basic Equivalent Circuits

To apply the equivalent circuit approach, the numerical values of the impedances Z_1 (R_1-C_1) and Z_2 (R_2-C_2-CPE) corresponding to the two structural areas of the films must be evaluated as follows: The impedance spectrum in a complex plane for the studied $SeSm_{0.008}$ is shown in Fig. (3) at temperatures 311, 250 and 100 K. Presence of one semicircle at each temperature in Fig. (3) means that we have two resistance where the higher one is more pronounced than the other. The experimental data shown in Fig. (3) are fitted using the most simple equivalent circuit $R_1 \| C_1$-$R_2 \| C_2$ (inset of Fig. (3)) which is represented numerically by following equations [15, 17]:

$$Z' = \frac{R_1}{1+(\omega R_1 C_1)^2} + \frac{R_2}{1+(\omega R_2 C_2)^2} \tag{3}$$

and

$$Z'' = \frac{\omega R_1^2 C_1}{1+(\omega R_1 C_1)^2} + \frac{\omega R_2^2 C_2}{1+(\omega R_2 C_2)^2} \tag{4}$$

The fitted points are plotted as short dashed lines where its extrapolation to *x*- axis gives the value of the higher resistance (R_1) at a given temperature.

The real, *M'*, and imaginary, *M''*, components, of the complex electric modulus *M** can be obtained from the following equations:

$$M' = \frac{C_o(\omega R_1 C_1)^2}{C_1[1+(\omega R_1 C_1)^2]} + \frac{C_o(\omega R_2 C_2)^2}{C_2[1+(\omega R_2 C_2)^2]} \tag{5}$$

$$M'' = \frac{C_o\omega R_1 C_1}{C_1[1+(\omega R_1 C_1)^2]} + \frac{C_o\omega R_2 C_2}{C_2[1+(\omega R_2 C_2)^2]} \tag{6}$$

The spectroscopic plot in Fig. (4), obtained at temperature T=311, 250 and 100 K for the studied $SeSm_{0.008}$ films, shows that the dependence of the imaginary components, *M''*, of the electric modulus has two peaks (Debye peaks) over the investigated frequency range. Furthermore, each peak of *M''*-log *f* corresponds to each of *RC* circuit. The maximum of these two peaks shifts to higher frequency as temperature decreases which means that the values of the capacitance of the two circuits depends on temperature. The frequency at the Debye peak maxima for each *RC* element and at each temperature is given by the expressions:

$$2\pi f_{1max} R_1 C_1 = 1 \tag{7}$$

$$2\pi f_{2max} R_2 C_2 = 1 \quad (8)$$

Since the value of R_1 is already obtained using Fig. (3), the values of the capacitance C_1 at different temperatures could be calculated using equation (7). The value of C_2 can be determined by using the spectroscopic plot of electric modulus in a complex plane, shown in Fig. (5). The spectrum in Fig. (5), calculated at 250 K, presents two incomplete semicircle arcs which means presence of two resistances R_1 and R_2 ($R_1 > R_2$ in the present case) and two capacitances C_1 and C_2. The experimental data in Fig. (5) are fitted using the simple circuit shown in the inset of Fig. (3) and equations (5) and (6). The intercept of the fitted curve, in Fig. (5), with M' axis can yield the value of C_2 as $M'(at\ point\ P) = \varepsilon_o(\frac{1}{C_1} + \frac{1}{C_2})$. By applying eq. (8) R_2 could be also determined.

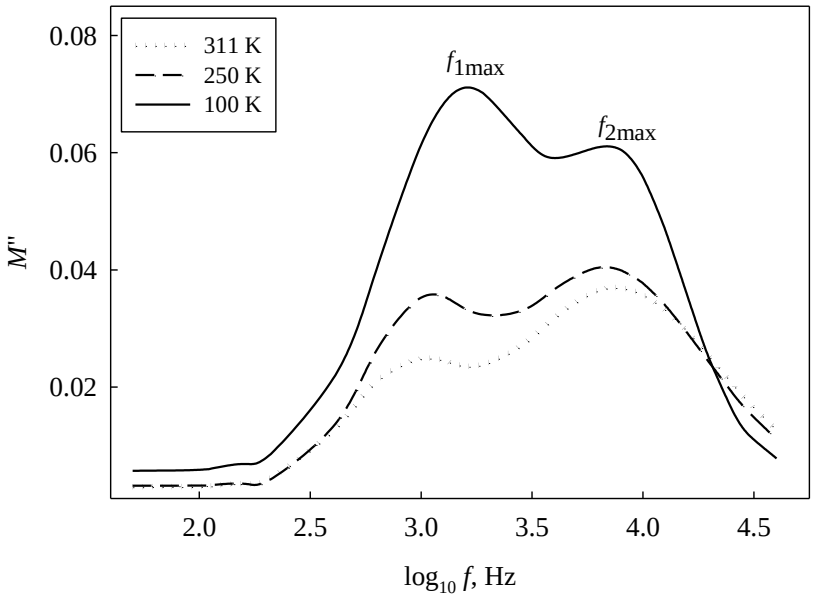

Figure (4). A plot of imaginary part of the electrical modulus, *M''*, as function of frequency for the studied $SeSm_{0.008}$ films at different temperatures

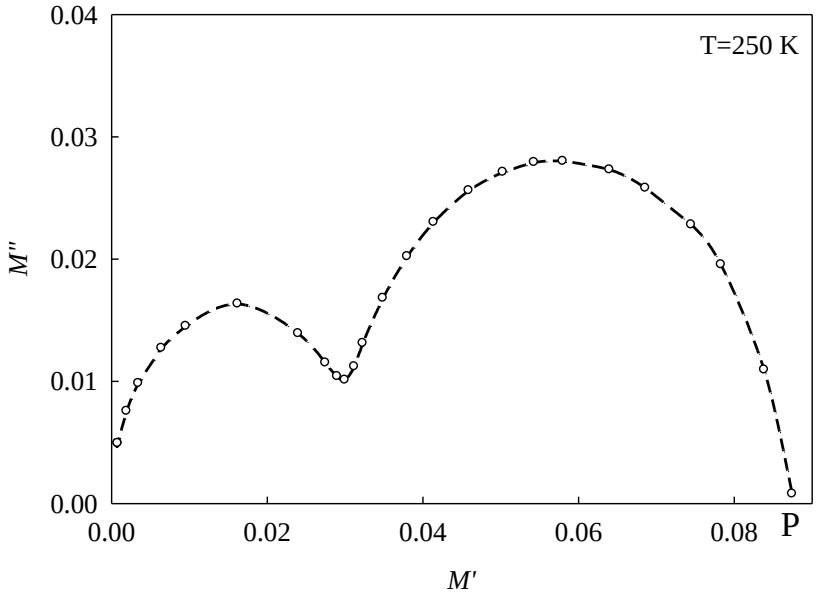

Figure (5). Spectroscopic plot of *M''* against *M'* at T=250 K. The symbols correspond to experimental data while dashed line represents the fitting using the equivalent circuit shown in the inset of Fig. (3) for the studied samples

3.3. Modeling of the Impedance Data Using Equivalent Circuit approach

Besides the basic circuit, with two parallel *RC* elements (inset of Fig. (3)), a more five equivalent circuits with CPE elements have been chosen for the purpose of modeling impedance characteristics for $SeSm_{0.008}$ thin films. The proposed electrical circuits are shown in Fig. (6) while the expression for total impedance *Z** for each circuit is given elsewhere [7, 18].

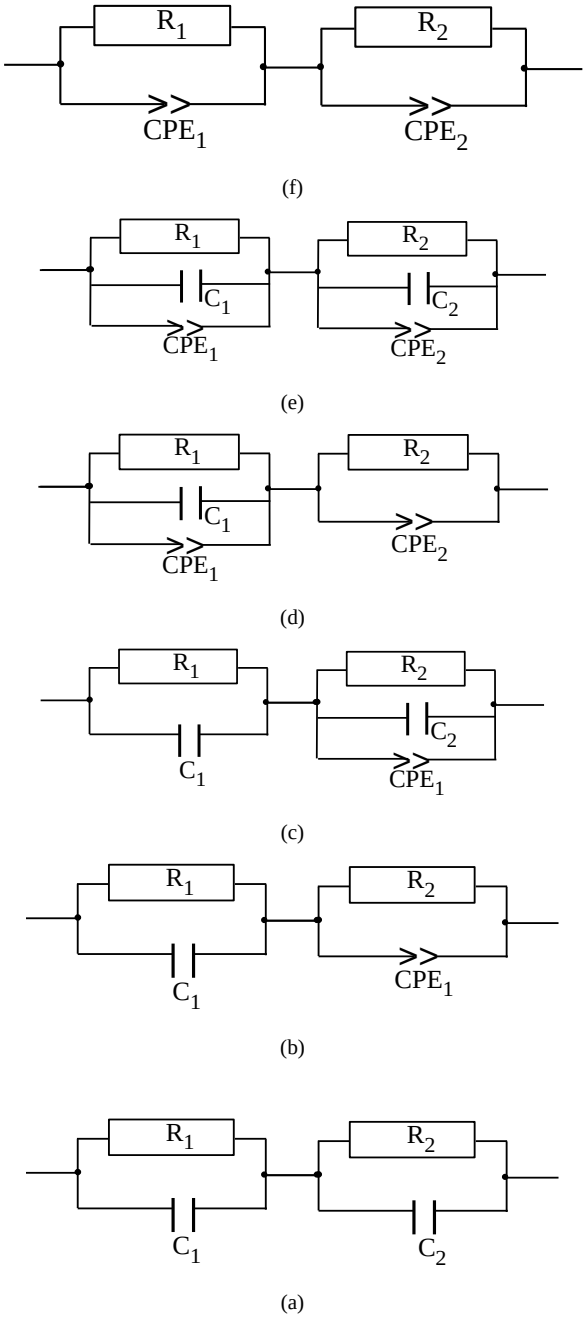

Figure (6). Various proposed equivalent circuits used to model IS data of the studied films

Considering the calculated initial values of the basic circuit elements R_1, R_2, C_1, C_2, n and A for the studied films (obtained in sec. 3.2), the theoretical and experimental data trends of the complex plot of *Z*'-*Z*'' (at 250 K), for all equivalent circuits, is shown in Fig. (7). Such a comparison reflects that the fitting using equivalent circuit number c which is composed of $R_1 \| C_1$ connected in series with $R_2 \| C_2 \| CPE_1$ and passes with the most points in Fig. (7) specially in the high frequency region is fairly good to represent the structure of the studied films over the whole investigated frequency range.

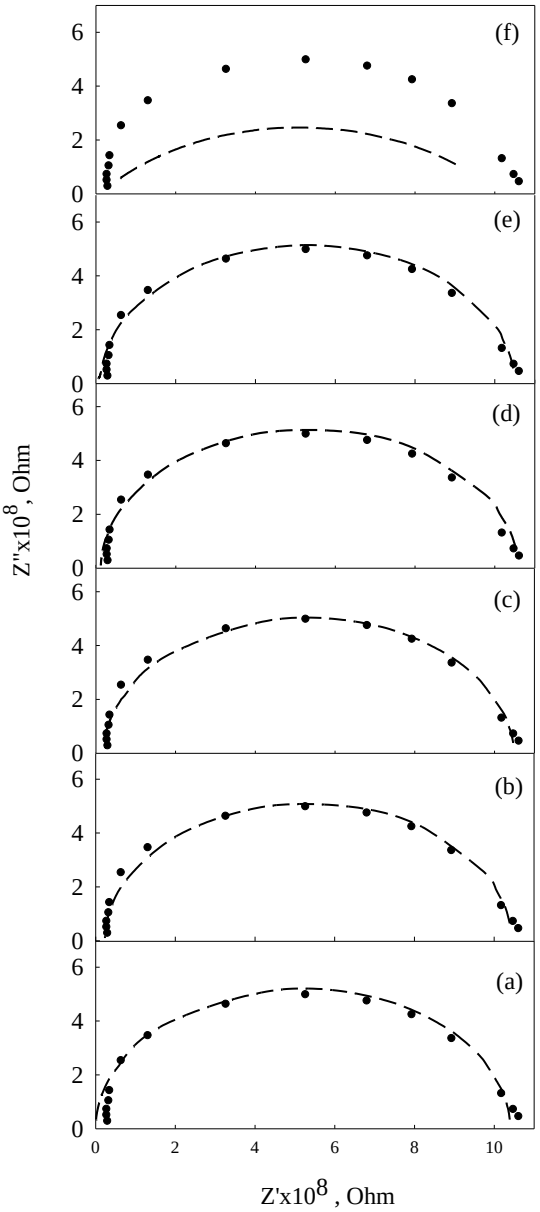

Figure (7). Measured (closed circles) and best fit (dashed lines) complex-plane impedance plots at 250 K for the present $SeSm_{0.008}$ films using the proposed equivalent circuits shown in Fig. (6). The sequence of the subfigures in Fig. (7) has the same meaning as in Fig. (6)

A critical test for the equivalent circuit model comes from the frequency dependence of the experimental data of the admittance *Y**. It should be noted that, Fig (2) shows just the real component of such plots in the investigated frequency

range. The values of *Y'* admittance in this figure in the low frequency range are depending on the temperature only while at higher frequency region it depends on both frequency and temperature. The experimental data of the real, *Y'*, and imaginary, *Y''*, components of the complex admittance Y^* together with its fitting curves for all equivalent circuits using the same fitting parameters used in Fig. (7) are shown in Fig. (8). From this figure it is observed that circuit c is the most suitable circuit to represent electrically both amorphous and crystalline structural phases of the studied film which ensures the obtained results from Fig. (7).

3.4. Investigation of Electrical Conduction Mechanisms

3.4.1. a.c. conduction

The fitting process to select the most appropriate circuit (sec. 3.3) yielded an adjustable and final value of the basic elements of circuit c (see figures 7 and 8). The values of the exponent *n* as calculated in the high frequency region of Fig. (2) and in the considered temperature range, is shown in Fig (9) as an open triangles.

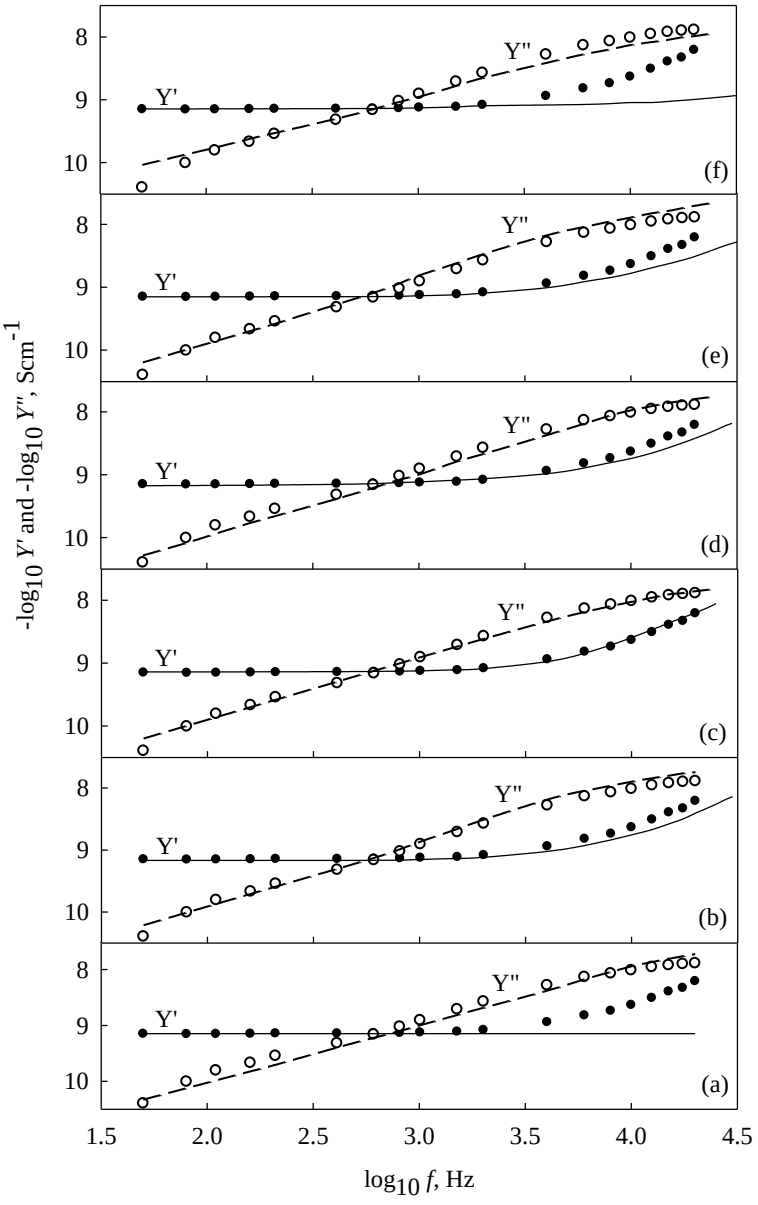

Figure (8). Measured *Y'* (solid circles), *Y''* (open circles) at 250 K and the best fit of *Y'* (solid lines) and *Y''* (dashed lines) spectroscopic plot as function of frequency for $SeSm_{0.008}$ films using the proposed equivalent circuits shown in Fig. (6). The sequence of the subfigures in Fig. (8) has the same meaning as in Fig. (6)

In the literature, various models have been proposed to explain the behavior of *n* which represents the exponent of Jonscher universal low for ac conductivity for semiconductors [19, 20]. These models differentiate between tunneling and hopping mechanisms. The tunneling which describes the overlap of the exponentially decaying wave function of the electrons due to its transition between two neighboring sites at a separation R are explained by simple quantum mechanical tunneling (QMT) [21], non-overlapping small polarons (NSPT) [21] and overlapping large polaron tunneling (OLPT) [22] models. On the other hand, "hopping" which is represented by correlated barrier (CBH) model, Elliott [23, 24] stated that for neighboring sites at a separation R, the Coulomb wells overlap, resulting in a lowering of the effective barrier height from W_M to a value W. Here the index *n* is evaluated as [23]:

$$n = 1 - \frac{6K_BT}{\left[W_M + K_BT\ln(\omega\tau_0)\right]} \quad (9)$$

Thus, in the CBH model a temperature dependent exponent *n* is predicted, with *n* increasing towards unity as $T \rightarrow 0.0$ K. More details about these conduction models are given elsewhere [21, 25].

Considering the studied temperature range and at typical values of the parameters $\tau_0 = 10^{-12}$ s, $\omega = 10^4$ s^{-1}, the theoretical trend of the function s = *f* (T) for the QMT model [21], NSPT model [21], OLPT model [22] and CBH model [23, 24] is shown in Fig. (9) together with the evaluated values of *n* in the present work $SeSm_{0.008}$. Such a comparison shows that the CBH model is fairly good to describe the a.c. conduction mechanism for the studied samples over the whole considerable temperature range. It should be noted that the previously calculated values of *n* for $SeSm_{0.005}$ films [12] are added to Fig. (9) for the sake of comparison. Figure (10) illustrate that CBH model as conduction mechanism is applicable also for other chalcogenide systems previously published in the literature for instance As_2Se_3 [26], As_2Se_3Ag [26], Se-Te-Sn [27], Ga-Se-Te [28] and also oxide glasses which behaves as semiconductor such as V_2O_5-Ge_2O, [25].

3.4.2. dc conduction

The adjustable and final values of the resistances R_1 and R_2 together with the thickness of the sample and contact area of the studied film are used to calculate the dc conductivity in the studied temperature range (311-100 K) as shown in Fig (11).

In case of calculated σ_{dc} using R_1, the plot of the function $\ln \sigma_{dc} = f(1/T)$ in Fig. (11), reveals presence of three distinct regions indicating three different conduction mechanisms and satisfies the following thermally activated conductivity relation [20]:

$$\sigma = \sigma_1 \exp(-\frac{\Delta E_1}{K_BT}) + \sigma_2 \exp(-\frac{\Delta E_2}{K_BT}) + \sigma_3 \exp(-\frac{\Delta E_3}{K_BT}) \quad (10)$$

where K_B is Boltzmann's constant. For each region, the function $\ln\sigma = f(1/T)$ is fitted locally point by point to the linear regression line with fitting parameter $R^2 \approx 0.99$. In the first region (311-240 K), the conduction mechanism is due to band-to- band electronic transition in the mobility gap with an activation energy ΔE_1. The conduction mechanism in the second region (240-150 K) is due to transition from valence band to the localized states of conduction band with activation energy of conduction ΔE_2. The third term corresponds to the third temperature region (150-100 K) which is due to hopping conduction near the Fermi level E_F. Furthermore, the dc conductivity calculated using R_2 and shown in Fig. (11) reveals presence of only two regions with two conduction mechanisms. These two regions lie in the temperature ranges 311-230 K and 230-100 K in sequence. The values of the characteristic electrical quantities, ΔE_1, ΔE_2 and ΔE_3 (thermal activation energies of conduction), σ_1, σ_2 and σ_3 (pre-exponential factors) and σ_{RT} (conductivity at room temperature ≈ 20 ℃) are listed in Table 1. For the sake of comparison the measured dc conductivity for the same $SeSm_{0.008}$ thin films is added to Fig. (11) while its characteristic electrical parameters are listed in Table (1).

The data shown in Fig. (11) together with its corresponding electrical quantities listed in Table (1) reflects that the conductivity calculated using R_1 and R_2 represents the amorphous and crystalline, in sequence, structural phases of the studied samples which is confirmed in the XRD pattern of Fig. (1).

The magnitude of C_1 and C_2 calculated using equivalent circuit approach vary in the ranges 0.5 $x10^{-12}$-$2.4x10^{-12}$ and 1.54 $x10^{-12}$-$2.70x10^{-12}$ Farad in sequence both in the temperature 311-100 K. This variation is found also in other chalcogenide compounds such as $Se_{85-x}Te_{15}Ge_x$ (x = 0, 2, 6, 10 and 15), [29], $Te_{50}As_{30}Ge_{10}Si_{10}$ [30], a-Sb_2Se_3 doped with Ag [31] and $Se_{70}Te_{30-x}Ag_x$ (x = 0-10) [32, 33].

Table (1). The characteristic electrical conductivity quantities $\Delta E_{1,2,3}$ (thermal activation energy of conduction), $\sigma_{1,2,3}$ (pre-exponential factor), σ_{RT} (conductivity at room temperature ~ 20 ℃) for the investigated $SeSm_{0.008}$ films. The corresponding values for the experimentally measured dc conductivity of the same films are also given for the sake of comparison

$SeSm_{0.008}$ films	ΔE_1, eV	ΔE_2, eV	ΔE_3, eV	-ln σ_1, ($\Omega.cm^{-1}$)	-ln σ_2, ($\Omega.cm^{-1}$)	-ln σ_3, ($\Omega.cm^{-1}$)	-ln σ_{RT}, ($\Omega.cm^{-1}$)
Amorphous phase	0.54	0.162	0.064	7.07	31.20	31.90	28.30
Crystalline phase	0.39	0.09	---	8.41	27.77	---	23.44
Measured films	0.56	0.17	0.07	7.90	29.90	32.10	29.40

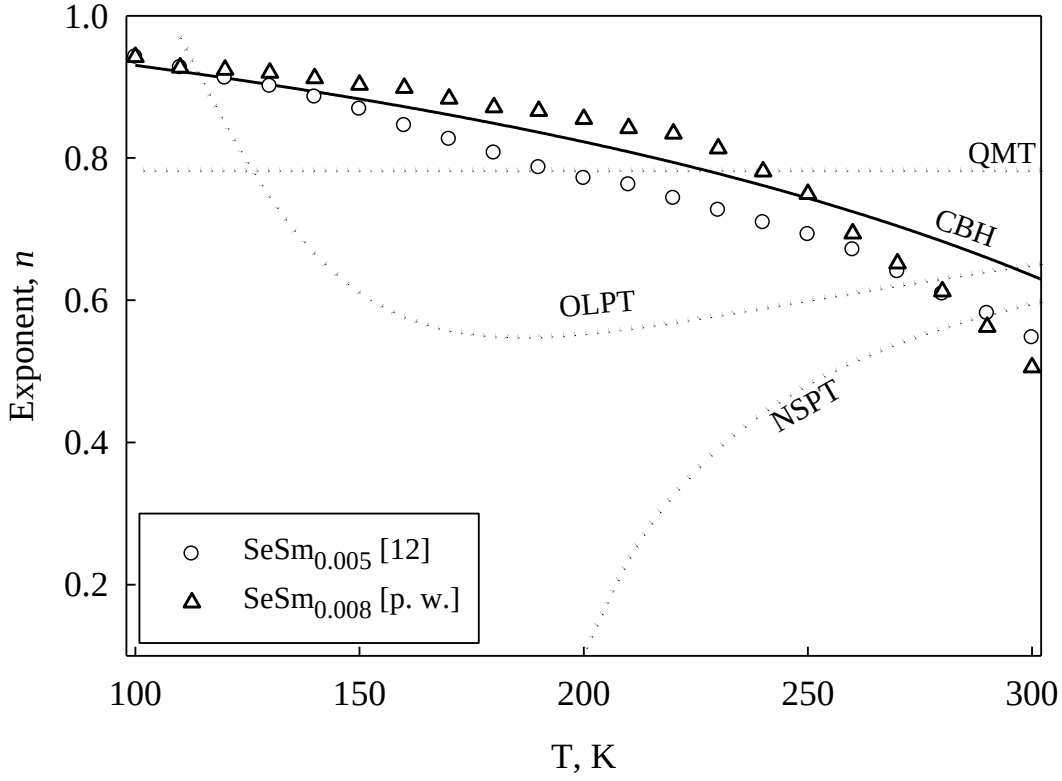

Figure (9). Temperature dependence of the frequency exponent *n* for the present work [p. w.], together with the previous published work [12]. The dotted curves represent the values calculated using the models: QMT [21], NSPT [21], OLPT [22] and CBH [23, 24]

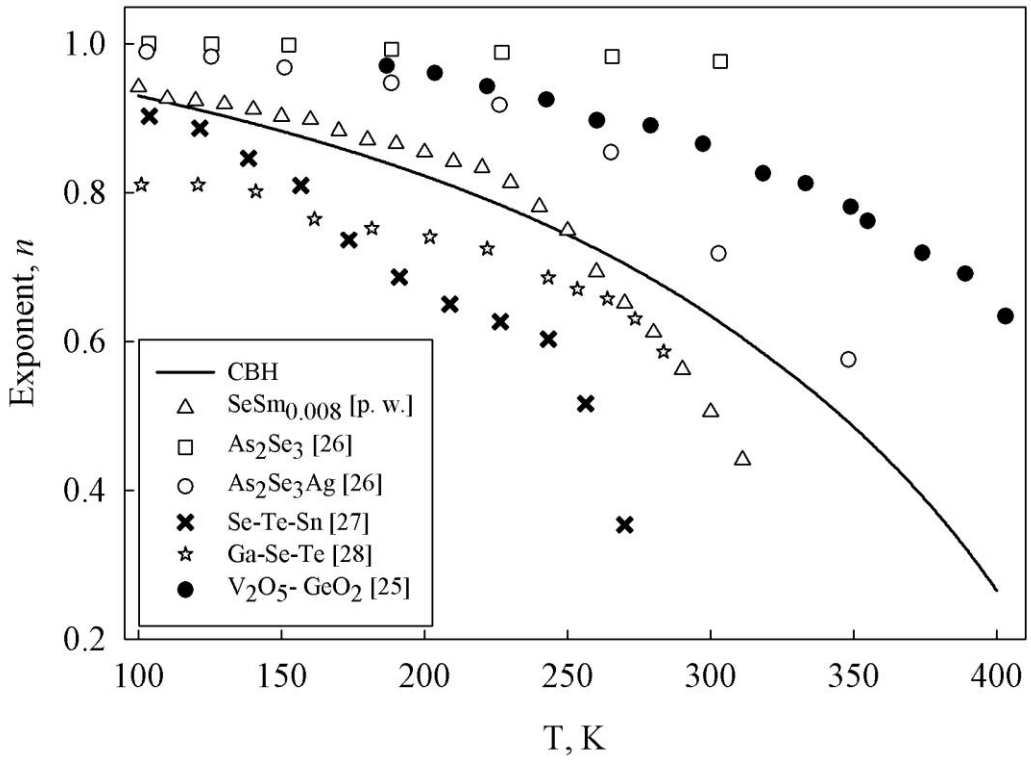

Figure (10). Temperature dependence of the frequency exponent *n* for the present work and other chalcogenide systems previously published in the literature for instance As_2Se_3 [26], As_2Se_3Ag [26], Se-Te-Sn [27], Ga-Se-Te [28] and also oxide glasses which behaves as semiconductor such as V_2O_5-GeO_2, [25]. The solid curve represents the theoretical values of *n* calculated using CBH model (Eq. 9))

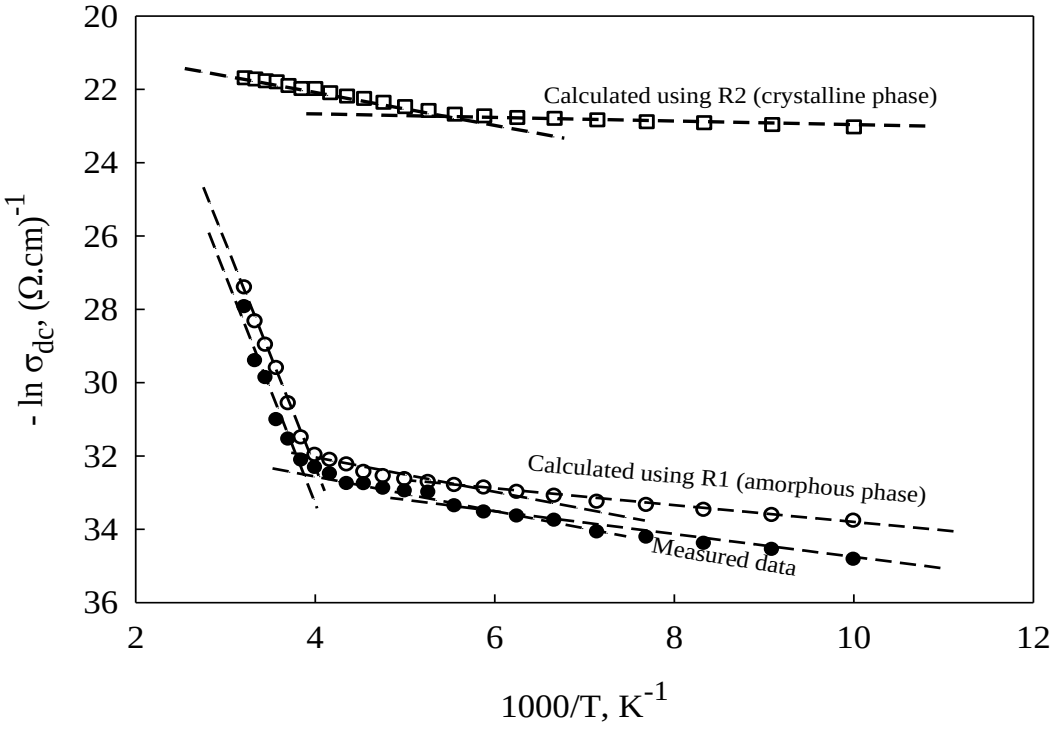

Figure (11). Temperature dependence of the dc conductivity, calculated using the amorphous, R_1, and crystalline, R_2, resistances for the present films. The measured conductivity of the same samples is also inserted in the figure for comparison. The symbols correspond to experimental data while dashed lines represent the fitting using linear regression

4. Conclusions

A detailed application of impedance spectroscopy approach on the effect of Sm doping to a-Se and polycrystalline $SeSm_{0.008}$ thin films, prepared by thermal evaporation, in the temperature 311–100 K and frequency 50 Hz–80 kHz ranges allows drawing the following conclusions:

1. The spectroscopic plot of the real part of the admittance as function of frequency showed an independent plateau (dc component) followed by a "cross over" region to high frequency dispersion (ac component) where log *Y*' increases linearly with log *f*. This trend illustrates presence of two micro-structure phases in the structural network of the studied film which is also confirmed by x-ray diffraction pattern.
2. In the low frequency section where Debye model is obeyed the microstructure are represented by $R \| C$ elementary circuit. Indeed, in the high frequency region the deviation from Debye trend is observed and the structure could be represented electrically by simple R ‖ C and constant phase element, CPE.
3. The complex plot of *Z*'-*Z*", *M*'-*M*" and *Z*",*M*" as function of the frequency are used to calculate the initial values of the basic elements of the circuits R_1, R_2, C_1, C_2 and impedance elements (*n* and *A)* for CPE.
4. A comparison between the theoretical values of the index *n* calculated using the current a.c. conduction models together with that obtained by applying the equivalent circuit approach in the high frequency range proved that correlated barrier hopping (CBH) is the most probable model to represent the a.c. conduction mechanism for the studied films.
5. Using the initial values as fitting parameters, the theoretical trend of the complex plot of *Z*'-*Z*" for all equivalent circuits together with the experimental results are calculated. Such a comparison revealed that equivalent circuit which is composed of $R_1 \| C_1$ connected in series with $R_2 \| C_2 \|$ CPE is fairly good to represent the micro-structure of the studied films over the whole studied frequency range.
6. The σ_{dc} of amorphous phase calculated using R_1 shows three distinct conduction while in the case of crystalline phase which is evaluated using R_2 shows only two conduction mechanisms.
7. The variation of the capacitances C_1 and C_2 lie in the limits (0.5-2.4) x 10^{-12} F and (1.54-2.7) x 10^{-12} F for amorphous and crystalline phases in sequences in the temperature 311-100 K. which is also observed in other chalcogenide compositions.

REFERENCES

[1] M. Kastner, Bonding bands, Lone pair bands and Impurity states in Chalcogenide Semiconductors, Phys. Rev. Lett. 28 (1972) 355-357.

[2] V.N. Antonov, B.N. Harmon and A.N. Yareska, Electronic structure of mixed-valence semiconductors in the LSDA+U approximation. I. Sm monochalcogenides, Phys. Rev. B 66 (2002) 165208-1-165208-10.

[3] H.S. Wio, B. Aloscio, and A. López, Phase diagram of samarium monochalcogenides, Sol. Stat. Commun. 15 (1974) 1933-1936.

[4] A. Svane, G. Santi, Z. Szotek, W.M. Temmerman, P. Strange, M. Horne, G. Vaitheeswaran, V. Kanchana, L. Petit and H. Winter, Electronic structure of Sm and Eu chalcogenides, Physica Status Solidi B 241 (2004) 3185-3192.

[5] B.G. Elmegreen, G. Bruce, K.L. Elbaum, L.X. Hu, J.G. Martyna, M. Muser, M.D. Newns, Piezo-driven non-volatile memory cell with hysteretic resistance, US patent application, Application Number: 12/234100, Filing Date: 09/19/2008.

[6] V. V. Kaminskii, S. M. Solov'ev, A. V. Golubkov, Electromotive Force Generation in Homogeneously Heated Semiconducting Samarium Monosulfide, Technical Physics Letters 28 (2002) 229-231.

[7] D. Mancic, V. Paunovic and Z. Petrušic, Application of Impedance Spectroscopy for Electrical Characterization of Ceramics Materials, Electronics 13 (2009) 11-17.

[8] D.C. Sinclair, Characterization of Electro-materials using ac Impedance Spectroscopy, Bol. Soc, Esp. Cerám. Vidrio 34 (1995) 55-65.

[9] V. Tudic, AC Impedance Spectroscopy of a-nc-Si:H Thin Films, Engineering 6 (2014) 449-461.

[10] E.J. Abram, D.C. Sinclair and A.R. West, A Strategy for Analysis and Modelling of Impedance Spectroscopy Data of Electroceramics: Doped Lanthanum Gallate J. Electroceramics 10 (2003) 165-177.

[11] F.A. Abdel-wahab, H.M. Maksoud and M.F. Kotkata, Electrical conduction and dielectric relaxation in semiconductor $SeSm_{0.005}$, J. Phys. D: Appl. Phys. 39 (2006) 190-195.

[12] M.F. Kotkata, F.A. Abdel-Wahab and H.M. Maksoud, Investigations of the conduction mechanism and relaxation properties of semiconductor Sm doped a-Se films, J. Phys. D: Appl. Phys. 39 (2006) 2059-2066.

[13] R. Suryanarayanan and C. Paparoditis, Preparation of rare earth chalcogenide thin films by the co-evaporation technique, J. Cryst. Growth 13/14 (1972) 389-392, ibid, Photoconductivity in SmSe, Phys. Lett A. 42 (1973) 373-374.

[14] R.B. Bekeen and J.W. Schweitzer, Intermediate valence in alloys of SmSe with SmAs, Phys. Rev. B 23 (1981) 3620-3626.

[15] A.R. West, D.C. Sinclair and N. Hirose, Characterization of Electrical Materials, Especially Ferroelectrics, by Impedance Spectroscopy, J. Electroceramics 1 (1997) 65-71.

[16] A.N Papathanassiou, The power law dependence of the a.c. conductivity on frequency in amorphous solids, J. Phys. D: Appl. Phys. 35 (2002) L88- L89.

[17] D.C. Sinclair and A.R. West, Impedance and modulus spectroscopy of semiconducting $BaTiO_3$ showing positive temperature coefficient of resistance, J. Appl. Phys. 66 (1989) 3850-3856.

[18] M.E. Orazen, B. Tribollet, Electrochemical impedance spectroscopy. John Wiley & Sons, Inc., USA, 2008.

[19] A.K. Jonscher, The universal dielectric response, Nature 267 (1977) 673-679.

[20] N.F. Mott and E.A. Davis, Electronic Processes in Non-Crystalline Materials, 2nd edn Clarendon Press, Oxford, 1979.

[21] A. Ghosh, Frequency-dependent conductivity in bismuth-vanadate glassy semiconductors, Phys. Rev. B 41 (1990) 1479-1488.

[22] R. Long, Frequency-dependent loss in amorphous semiconductors, Adv. Phys. 31 (1982) 553-637.

[23] S.R. Elliot, A.c. conduction in amorphous chalcogenide and pnictide semiconductors, Adv. Phys. 36 (1987) 135-218.

[24] S.R. Eilliot, A theory of a.c. conduction in chalcogenide glasses, Phil. Mag. B 36 (1977) 1291-1304.

[25] A. Ghosh, Transport properties of Vanadium germanate glassy semiconductors, Phys. Rev. B 42 (1990) 5665.

[26] F. Abdel-Wahab, Signature of the Meyer–Neldel rule on the correlated barrier-hopping model, J. Appl. Phys. 91 (2002) 265-270.

[27] F. Abdel-Wahab, A.A. Montaser, A. Yelon, Mechanism of ac and dc conduction in chalcogenide glasses, Monatsh Chem. 144 (2013) 83–89.

[28] A.S. Maan, D.R. Goyal and A. Kumar, A.C. conductivity of amorphous Ga-Se-Te system, Revue De Phys. Appl. 24 (1989)1071-1075.

[29] A. Kumar, M. Lal, K. Sharma, P.S. Gill, and N. Goyal, Dielectric properties of $Se_{85-x}Te_{15}Ge_x$ chalcogenide glasses, chalcogen Lett. 11 (2014) 249-256.

[30] T. Suntola, O.J.A. Tiainen and M. Valkiainen, Differential capacitance of chalcogenide thin films, Thin Solid Films 14 (1972) S3-S5.

[31] S. Gautam, A.Thakur, S.K. Tripathi and V. Goyal, Effect of silver doping on the electrical properties od a-Sb_2Se_3, J. Non-Cryst. Solids 353 (13-15) (2007) 1315-1321.

[32] N. Chaoudhary and A. Kumar, Dielectric relaxation in glassy $Se_{70}Te_{30-x}Ag_x$, Indian J. Pur. & Appl. Phys. 44 (2006) 62-65.

[33] S. Wagle and V. Shirodkar, Dielectric Properties of thin Film Al/$Sb_2Pb_1Se_7$/Al Devices, Brazil. J. of Phys. 30 (2000) 554-559.